A new device for high-resolution Li K X-ray spectroscopy using an electron microprobe

Pia Schweizer, Emmanuelle Brackx, Philippe Jonnard

Spectrochimica Acta Part B: Atomic Spectroscopy 218 (2024) 106994

Contents lists available at ScienceDirect

Spectrochimica Acta Part B: Atomic Spectroscopy

journal homepage: www.elsevier.com/locate/sab

A new device for high-resolution Li K X-ray spectroscopy using an electron microprobe

Pia Schweizer [a,b,*], Emmanuelle Brackx [a], Philippe Jonnard [b]

[a] CEA, DES, ISEC, DMRC, Univ Montpellier, Marcoule, France
[b] Laboratoire de Chimie Physique—Matière et Rayonnement, Faculté des Sciences et Ingénierie, Sorbonne Université, UMR CNRS, 4 place Jussieu, 75252 Paris Cedex 05, France

ARTICLE INFO

Keywords:
Lithium detection
Electron microprobe
Multilayers
Microanalysis

ABSTRACT

Lithium is one of the key elements in today's materials and battery industry, and the interest in non-destructive characterization techniques at a micron scale for materials containing lithium is steadily increasing. The electron microprobe is a reliable and accessible analysis tool widely used for this purpose, but performing X-ray emission spectroscopy in the low-energy range is still challenging.

In this work, we demonstrate that spectroscopy in the Li K energy range is feasible by integrating a new detection system composed of a multilayer and ultra-thin separation windows into a commercial wavelength dispersive spectrometer of a microprobe. The detection system is described in detail, and the results, in form of spectra showing the Li K emission in LiF and in a ternary quasicrystalline sample, are presented and analyzed. In LiF the emission band is centered at 54.5 eV and has varying intensities for different beam exposure times. The spectra obtained in the ternary quasicrystal clearly demonstrate that the detection system has sufficient energy resolution to separate the Li emission band and the Al $L_{2,3}$ and Cu $M_{2,3}$ emission bands, enabling chemical state analysis by comparing the shapes of the emissions. To our knowledge, this is the first time such a detection system, implemented in a WDS spectrometer and enabling the acquisition of different Li K spectra in various compounds has been described in detail. This kind of system can be used for Li quantification using a common procedure in electron probe microanalysis.

1. Introduction

Soft X-ray spectroscopy is a reliable technique for non-destructive and accurate material characterization. The electron microprobe, based on wavelength-dispersive spectrometry (WDS), is widely used for both scientific and industrial applications. Since the beginning of electron probe microanalysis (EPMA) introduced by Raimond Castaing in 1951 [1], significant progress has been made in analyzing light elements [2–4]. However, despite the great interest in lithium (Li), particularly in the energy sector [5,6], and the urgent need for accurate non-destructive analysis at a micron scale to enable, for example, in situ measurements on batteries, detecting Li with an electron microprobe equipped with a bent crystal spectrometer and multilayers remains challenging. Recently developed periodic multilayers allow spectroscopy in the energy range around the characteristic Li emission (~ 50 eV) [7,8]. Some acquisitions of spectra showing the Li Kα emission using a scanning electron microscope or an electron microprobe equipped with a diffraction grating have already been published [9–11]. Other non-destructive techniques, such as X-ray photoelectron spectroscopy (XPS), allow for Li detection. However, XPS is extremely surface-sensitive, with analysis depths of less than ten nm, whereas the electron microprobe can analyze thicknesses of up to several hundred nm, depending on the material.

Nevertheless, scientists encounter difficulties when trying to detect Li through soft X-ray emission spectroscopy (SXES) due to various factors. The fluorescence yield of Li is extremely low, resulting in the production of few characteristic photons during the deexcitation process of Li atoms, which favors the emission of Auger electrons [12]. As a result of their low energy, the photons undergo strong auto-absorption by the sample and sample coating. Consequently, the signal originates principally from a thin surface layer, often degraded by contamination and sensitive to electron bombardment. Additionally, further photon absorption by the microprobe components, especially by separation windows, decreases the measured signal intensity.

Since the Li K emission (2p – 1 s transition) involves valence

* Corresponding author at: CEA, DES, ISEC, DMRC, Univ Montpellier, Marcoule, France.
E-mail address: pia.schweizer@cea.fr (P. Schweizer).

https://doi.org/10.1016/j.sab.2024.106994
Received 23 May 2024; Received in revised form 11 July 2024; Accepted 11 July 2024
Available online 15 July 2024

electrons, the shape of the Li emission band is highly dependent on the density of states (DOS) of the valence band and thus highly dependent on the chemical state of the Li atom. Chemical shifts of some eV and strong peak shape alterations can occur and should be expected for EPMA of light elements, [13,14], complicating quantitative analysis.

This work specifies, to our knowledge for the first time, a detection system implemented in a commercial WDS spectrometer of an electron microprobe which allows the detection of the Li Kα emission in different materials with Li concentrations down to 9% [15]. The new device includes a specially developed multilayer and ultra-thin low-absorbing separation windows. A description of the device and the analyzed materials is found in section 2. We demonstrate that this system is well-suited to resolve Li signal from possible overlapping contributions of other heavier elements showing characteristic emission bands in the same spectral range as Li. The aim of this article is to present this new technique, which is more accessible than other techniques using synchrotron radiation, and less onerous than detection using a scanning electron microscope (SEM) equipped with multilayer gratings.

2. Materials and methods

2.1. Electron microprobe

A classical electron microprobe includes several components such as the electron gun, electron lenses, the sample holder, energy- or wavelength dispersive spectrometers and a backscattered electron detector [16] where there are some differences in the setup among the three main manufacturers, CAMECA, JEOL and Shimadzu. For all instruments, the basic working principle is as follows: the sample, placed in the object chamber, is bombarded by the electron beam produced from the electron gun and aligned in the tube. This leads to the emission of various signals, e.g. secondary electrons, backscattered electrons, Auger electrons, and X-rays.

When the electron beam's energy exceeds the critical energy required to ionize the sample's atoms, characteristic X-rays produced by the deexcitation process are emitted. When using wavelength dispersive spectrometers, the photons entering the spectrometer are diffracted according to Bragg's law by natural crystals or multilayers and subsequently detected by a proportional counter. The measured spectrum is a superposition of the characteristic emission peaks and a continuous signal. This continuous background is composed of Bremsstrahlung and photons resulting from the total reflection of the dispersive element. For multilayers, the background intensity caused by total reflection varies inversely with the fourth power of the sine of the glancing angle. The sample, the dispersive element, and the proportional counter are constantly kept on a focussed circle, the so-called Rowland circle. The object chamber and the tube are kept under a secondary vacuum, while the spectrometers operate under a primary vacuum.

For this study, we used a CAMECA SXFive FE TACTIS microprobe that has five spectrometers with up to four dispersive elements to enable parallel detection of photons across different energy ranges. The Rowland circle diameter is 320 mm, large enough that there are no further collimating slits required to achieve optimal spectral resolution. Photons diffracted by the multilayers are detected using a proportional counter filled with a mixture of argon/methane gas. The spectrometers are either equipped with high or low-pressure detectors.

Due to variations in vacuum levels among chambers, thin separation windows are installed at the interfaces between the main chamber, where the specimen is placed, and the spectrometer, as well as between the spectrometer and the proportional counter.

After years of research on multilayers suitable for extreme ultraviolet lithography as well as research on solar physics [17], multilayers of types such as Si/Mo, Si/B_4C, and Si/SiC should allow the reflection of characteristic X-rays in the lithium spectral range (~ 25 nm). Moreover, recent studies on a newly developed multilayer composed of the light elements Be/Si/Al demonstrate high reflection around the Li K emission [7]. Another multilayer allowing the diffraction of photons at this energy has been integrated into a spectrometer of the microprobe [15]. This bent multilayer is composed of periodically alternating thin layers of boron and silicon with a total stacking period of 20.5 nm. Reflectivity calculations using IMD [18] software enable the performance of this multilayer to be assessed. Fig. 1 shows the reflectivity curve for a fixed Bragg angle of 40.2°, corresponding to the position of the Li K emission, in function of the photon energy. One can see that the reflectance at 54 eV is 15% with a bandwith of 4 eV.

Implemented into the Rowland circle low-pressure spectrometer (1 bar), the multilayer's analysis domain ranges from 45 eV to 130 eV and should allow the detection of the emission bands from Mg $L_{2,3}$ to P $L_{2,3}$, including the M emission bands of transition metals.

New spectrometry techniques at very low energies also require the development of new separation windows that are transparent to radiation in this energy range. Traditionally used windows, typically made of several micrometer thick layers of beryllium, offer the advantage of being highly resistant and nearly transparent to hard X-rays. However, below 1 keV, they become highly absorbent, leading to the use of polymer windows made of polypropylene or BoPET, with thicknesses ranging from some tens of micrometers to a few micrometers. Yet, below a few hundred eV, X-ray absorption by these windows also becomes a limiting factor in the analysis, necessitating the use of alternative window materials to improve detection limits. Ultra-thin windows made of silicon nitride (SiN) have been under investigation for some years now and have demonstrated excellent performance, particularly in XRF applications [20]. Further details about the manufacturing process and their characteristics are provided in the following paragraph.

The windows are manufactured through low-pressure chemical vapor deposition. An ultra-thin film of 20 nm SiN is deposited on a thin polycrystalline silicon grid. One or both sides of the window can be coated with thin metal layers, typically a few nm thick, applied either through sputtering or electron beam physical vapor deposition. This coating serves to filter out unwanted radiation and render the structure conductive, which is essential if the windows are used as a separation between the proportional counter and the spectrometer chamber. Fig. 2 shows an illustration of such a separation window and its support grid.

The hexagonal silicon grid, covering approximately 20% of the window surface, helps to stabilise the structure. Notably, the window can withstand pressure differences of up to 5 bar [20]. Fig. 3 presents a comparison of the X-ray transmission up to 2000 eV for the window types that are mainly used for low-energy applications.

Two of these windows were integrated in the microprobe at the interface between the main chamber and the spectrometer equipped

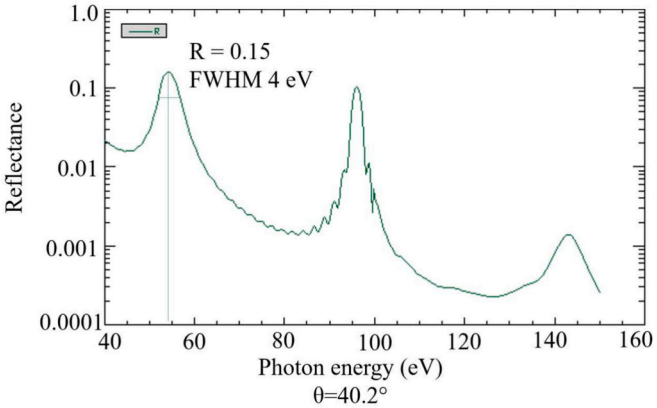

Fig. 1. Reflectivity curve for the B/Si multilayer at a fixed Bragg angle of 40.2° in function of the photon energy. A roughness of 0.5 nm was considered at each interface and the attenuation coefficients used for the simulation are taken from CXRO [19]. One can see that the reflectance at 54 eV is 15% with a bandwith of 4 eV. Further, higher diffraction orders may not be neglected.

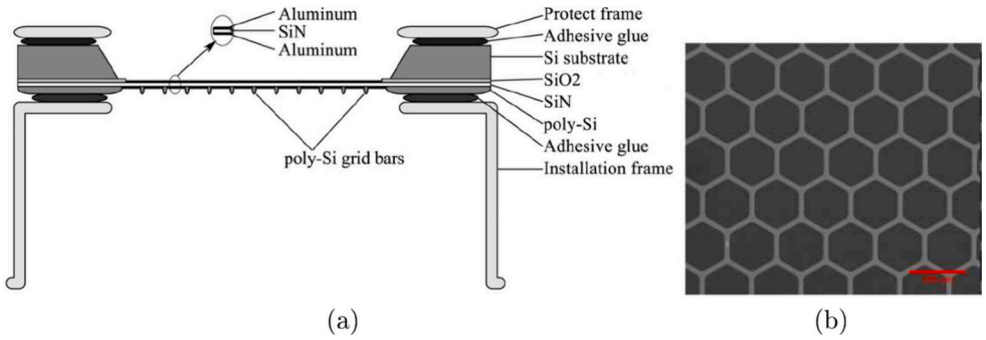

Fig. 2. (a) Illustration of the structure of an ultra-thin SiN window [20]; (b) SEM image of the support grid for SiN windows [21].

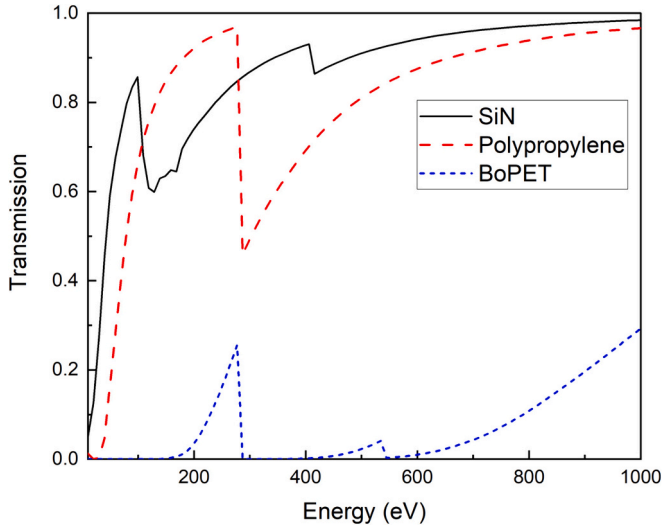

Fig. 3. X-ray transmission curve for photons below 1000 eV for ultra-thin windows made of SiN (20 nm), polypropylene (0.2 μm) and BoPET (3 μm); the data used for the transmission calculations comes from CXRO [19]. Especially at extreme low energies, below 100 eV, the SiN window shows better transmission properties.

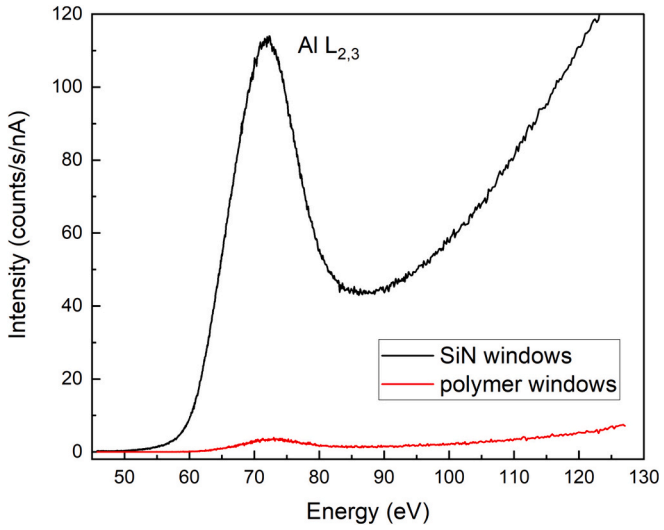

Fig. 4. Comparison of the acquisitions on a pure Al sample with the spectrometer equipped with polymer windows and ultra-thin SiN windows. With the ultra-thin windows, the detected intensity is about 30 times higher than with the standard commercialised polymer windows.

with the new multilayer, as well as between the spectrometer and the proportional counter. Subsequent tests conducted on a pure aluminium (Al) sample measuring the X-ray Al $L_{2,3}$ emission at 72.5 eV [22] indicate that the absorption caused by the new, thinner separation windows is about 30 times less important at 72 eV (see Fig. 4).

2.2. Analyzed samples

Li measurements were conducted on two bulk samples: lithium fluoride (LiF) with 26.8 wt% of Li and a quasicrystalline sample, containing phases with varying amounts of Al, copper (Cu) and Li. As the LiF sample is non-conductive, the sample contour was coated with a conductive gold paint. The quasicrystalline sample was mounted in a conductive resin with carbon filler.

As shown in Fig. 4 the new ultra-soft X-ray detection systems allows the measurement of the L emission band of Al. It is also possible to detect the M emission band of some transition metals of the fourth period, such as Cu.

2.3. Analysis conditions

The microprobe settings and its electronics were optimized to maximize the signal for Li emission. The acquisitions were carried out over the whole energy range of the crystal, with 1000 steps and a dwell time of 0.8 s/channel.

Prior to each acquisition, the electron beam alignment was optimized by focusing it onto a spot with 1 μm diameter on the sample surface. Measurements were conducted at different beam currents, reaching up to 700 nA, with an acceleration voltage of 5 kV. This voltage was determined using theoretical calculations performed by Monte Carlo simulations with CASINO ('monte CArlo SImulation of electroN trajectory in sOlids') [23], see Fig. 5(a). Similar work has been carried out by Hovington et al. [24]. One observes that the intensity is maximum for low acceleration voltages. Nonetheless, the measurement at 5 kV is much more convenient as the microprobe is closer to its optimal working conditions. It turned out that the measured intensity of the Li emission in LiF with an acceleration voltage of 5 kV was higher than at lower voltages. One possible explanation could be that the measurement is more sensitive to surface effects at low voltages. The calculated attenuation length for Li Kα photons in LiF is only 21 nm, whereas for other materials, it is one or two orders of magnitude higher, as illustrated in Fig. 5(b).

3. Results and discussion

3.1. LiF

The spectrum acquired on the LiF sample, shown in Fig. 6, allowed the detection of an intense emission band centered at 54.5 eV, consistent with findings by Takahashi et al. [25]. One can observe that higher beam currents and longer surface exposure times result in a more intense

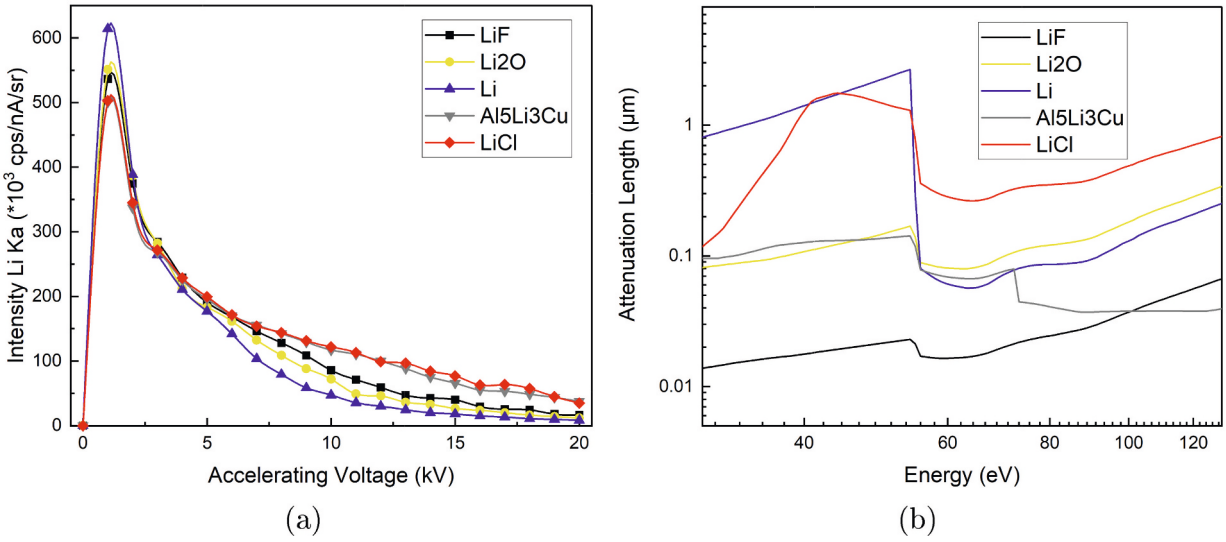

Fig. 5. (a) Li Kα line intensity for different materials as a function of acceleration voltage. Monte Carlo calculations are made with the CASINO software [24]; (b) Attenuation lengths for photons with an energy between 30 eV and 130 eV for different materials [19].

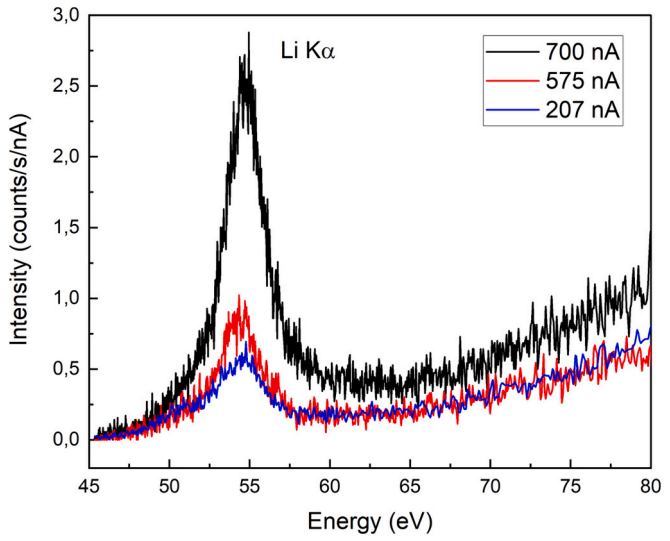

Fig. 6. Acquired spectra on LiF with different beam currents showing the Li Kα emission at an energy of 54.5 eV.

emission. It is well-known that halogens migrate under electron bombardment, leading to partial removal of fluorine and accumulation of lithium metal on the sample surface. Therefore, this band is attributed to the Li Kα emission from Li metal, with a tabulated energy of 54.25 eV [22]. The spectra show a slight assymetry, most notable in the 207 nA acquisition, on the low-energy side of the emission band. This assymetry could be due to the presence of an emission of lithium oxide (Li_2O), observed around 48 eV (Li_2O) [26–28].

The FWHM of the intense Li oxide emission is 4 eV which corresponds to the sum of the Gaussian broadening caused by the multilayer and the natural width of the emission band. This energy resolution is sufficient for detecting Li emission undergoing chemical shifts in function of its chemical state and for separating emission lines from heavier elements. However, the resolution of the multilayer is insufficient to distinctly seperate the two contributions coming from Li metal and Li_2O.

3.2. Quasicrystal

The quasicrystalline sample contains different phases composed of Al, Cu and Li. Detailed discussions on the formation of ternary quasicrystals containing Al can be found in [29–31]. In total, seven compounds exist, with the most significant being T_1 (Al_2CuLi), T_2 (Al_6CuLi_3) and T_B ($Al_{15}Cu_8Li_3$). The designation and composition of these seven phases are listed in Table 1. Prior to EPMA analysis, the sample was investigated using X-ray diffraction (XRD), scanning electron microscopy, and electron backscatter diffraction (EBSD). These analysis revealed the presence of phases T_1, T_2 and a phase consisting mainly of Al, likely the phase δ'. Fig. 7 shows a SEM image of the entire sample and a zoomed-in view on the discussed phases.

For the quasicrystalline sample, all acquisitions were carried out at 5 kV and 200 nA to prevent saturation of the detection system, given the high intensity of the Al $L_{2,3}$ emission. WDS spectra acquisitions were performed on the phases δ', T_1, and T_2, as shown in Fig. 8(a). One can observe the intense Al $L_{2,3}$ emission band of the δ' phase that contains a high amount of Al. On the other two spectra, one also observes a less intense emission band at the energy position of the Al $L_{2,3}$ transition. This peak results from the superposition of the contributions from the Al $L_{2,3}$ and the Cu $M_{2,3}$ transitions at 72.5 eV and 74.3 eV respectively. The slightly different shape of the emission band is due to the different concentrations of Al and Cu in the two phases. The T_1 phase contains

Table 1
Nomenclature, mass fraction and crystal structure of the different phases [29].

phase	composition	mass fraction	crystal structure
δ'	Al_3Li	Al: 0.9210 Li: 0.0790	Ll_2
δ	AlLi	Al: 0.7954 Li: 0.2046	B_{32}
Θ'	Al_2Cu	Al: 0.4592 Cu: 0.5408	tetragonal
T_1	Al_2CuLi	Al: 0.4336 Cu: 0.5106 Li: 0.0558	hexagonal
T_B	$Al_{15}Cu_8Li_2$	Al: 0.4366 Cu: 0.5484 Li: 0.0150	cubic
T_2	Al_6CuLi_3	Al: 0.6574 Cu: 0.2580 Li: 0.0846	icosahedral
R	Al_5CuLi_3	Al: 0.6152 Cu: 0.2898 Li: 0.0950	cubic

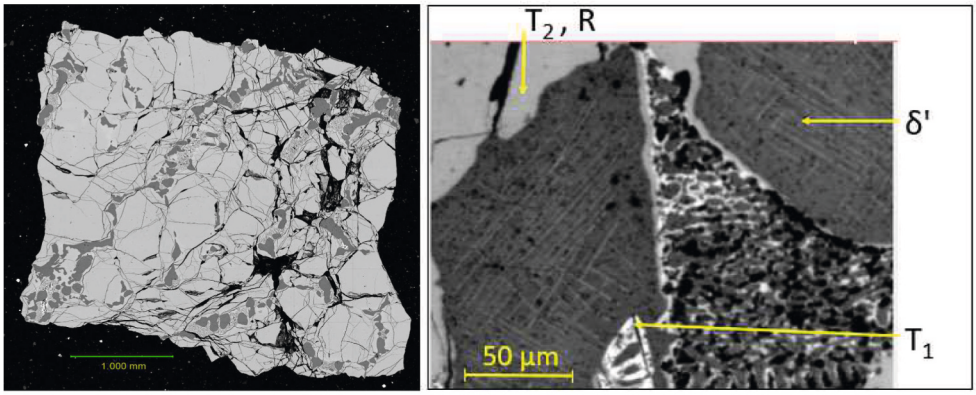

Fig. 7. SEM images of the quasicrystalline sample. The composition of the three different phases is listed in Table 1.

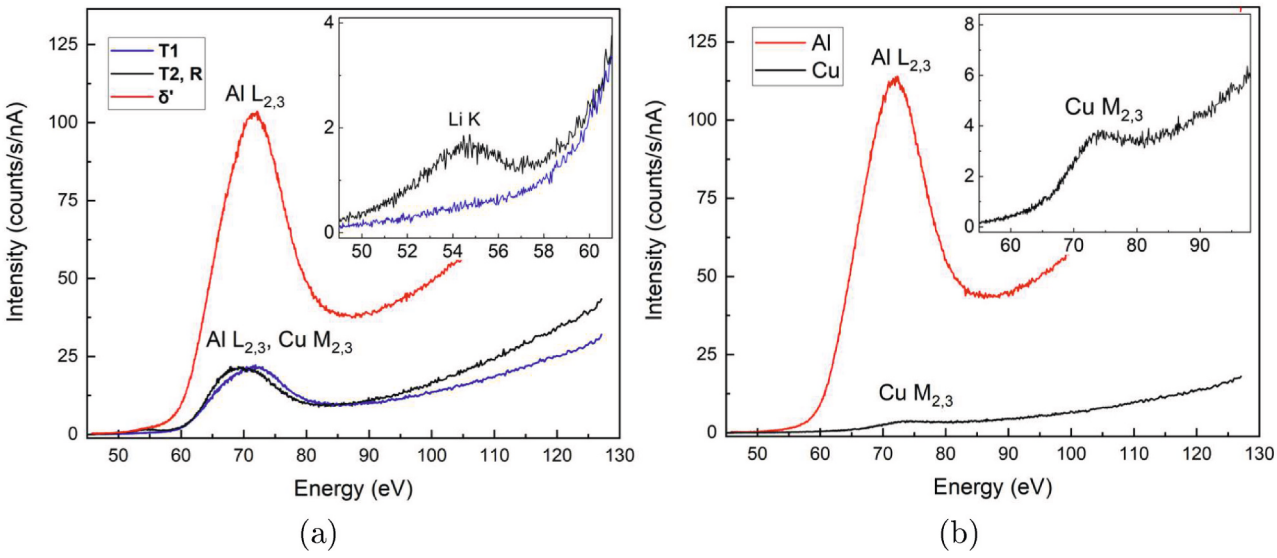

Fig. 8. (a) WDS spectra of the phases δ', T_1 and T_2; (b) Acquisitions on pure Al and Cu samples showing the Al $L_{2,3}$ emission and the Cu $M_{2,3}$ emission.

more Cu and its maximum shifts to a slightly higher energy, according to the energy difference between the Al $L_{2,3}$ and Cu $M_{2,3}$ transition. For comparison, Fig. 8(b) presents the acquisitions on a pure Al and a pure Cu sample.

The zoom on Fig. 8(a) shows the Li K emission band, only observed for the T_2 phase with the highest Li mass fraction. Given that the electronic states of aluminium oxide may extend down to 52 eV [13], we conducted WDS measurement on Al_2O_3 to confirm that the observed emission is not caused by the Al $L_{2,3}$ transition but by the Li K transition. In our case, the emission from Al_2O_3 is observed above 60 eV. One might expect to see the Li K emission band for the δ' phase, which has only a slightly lower Li concentration than the T_2 phase. Nevertheless, the extremely intense Al $L_{2,3}$ emission band drowns out the Li K intensity.

Similar to LiF, the maximum of the Li emission in the quasicrystalline sample is found at 54.5 eV, and the emission can be attributed to lithium metal. Nevertheless, despite the similarity in energy position to that observed for the LiF sample, its form differs from the Li Kα emission band shown in Fig. 6 and remains stable even with longer surface beam exposure times.

4. Conclusion

The integration of recently developed multilayers and ultra-thin separation windows into a WDS Rowland circle spectrometer of an electron microprobe allows for the detection of the Li Kα emission in different Li compounds. This advance is of great interest given the importance of lithium as a key element in today's industry and the persistent challenges in its analysis. The electron microprobe is a powerful tool with excellent spatial resolution and sufficient resolving power to separate the Li K signal from possible overlapping contributions of other elements. Compared to microprobes equipped with grating spectrometers, which have even better energy resolution [32], the WDS Rowland circle setup allows for accurate non-destructive quantitative analysis by performing quantification simultaneously on different spectrometers. This capability addresses the urgent need for a reliable and accessible technique for quantifying Li in battery materials, ceramics, and materials used in the aerospace sector, among others.

However, it's worth noting that the measured intensity remains low and Li spectroscopy using WDS EPMA requires high beam currents that can damage the sample, as it is the case for LiF. Nonetheless, the stable behavior observed in other samples holds promise for quantitative analysis. Recent work on Li quantification by EPMA has been presented [33,34] and further work is on the way.

CRediT authorship contribution statement

Pia Schweizer: Writing – original draft, Investigation, Formal

analysis, Conceptualization. **Emmanuelle Brackx:** Supervision, Resources, Funding acquisition, Conceptualization. **Philippe Jonnard:** Writing – review & editing, Validation, Supervision, Conceptualization.

Declaration of competing interest

The authors declare that they have no known competing financial interests or personal relationships that could have appeared to influence the work reported in this paper.

Data availability

Data will be made available on request.

Acknowledgements

Financial support from the CEA cross-cutting basic research Program RBNEW is gratefully acknowledged.

References

[1] C. Colliex, The “father” of microanalysis: Raymond Castaing, creator of a generation of scientific instruments, still in worldwide operation, C. R. Phys. 20 (7–8) (2019) 746–755. ISSN 1631-0705,, https://doi.org/10.1016/j.crhy.2018.12.001.
[2] P. Schweizer, E. Brackx, P. Jonnard, Electron probe microanalysis of light elements: improvements in the measurement and signal extraction methods, X-Ray Spectrom. (2022) 1, https://doi.org/10.1002/xrs.3290.
[3] S.-Y. Yang, S.-Y. Jiang, Q. Mao, Z.-Y. Chen, C. Rao, X.-L. Li, W.-C. Li, W.-Q. Yang, P.-L. He, X. Li, Electron probe microanalysis in geosciences: analytical procedures and recent advances, At. Spectrosc. 43 (2) (2022) 186–200. ISSN 0195–5373, 10.46770/AS.2021.912.
[4] X. Llovet, A. Moy, P.T. Pinard, J.H. Fournelle, Electron probe microanalysis: a review of recent developments and applications in materials science and engineering, Prog. Mater. Sci. 116 (2021) 100673. ISSN 0079-6425, https://doi.org/10.1016/j.pmatsci.2020.100673.
[5] P.K. Choubey, M.-S. Kim, R.R. Srivastava, J.-C. Lee, J.-Y. Lee, Advance review on the exploitation of the prominent energy-storage element: Lithium. Part I: from mineral and brine resources, Miner. Eng. 89 (2016) 119–137. ISSN 0892-6875,, https://doi.org/10.1016/j.mineng.2016.01.010.
[6] C. Dessemond, F. Lajoie-Leroux, G. Soucy, N. Laroche, J.-F. Magnan, Spodumene: the lithium market, resources and processes, Minerals 9 (2019) 334, https://doi.org/10.3390/min9060334.
[7] V. Polkonikov, N. Chkhalo, R. Pleshkov, A. Giglia, N. Rividi, E. Brackx, K. Le Guen, I. Ismail, P. Jonnard, Periodic multilayer for X-ray spectroscopy in the Li K range, Appl. Sci. 11 (2021) 6385, https://doi.org/10.3390/app11146385.
[8] K. Hassebi, E. Meltchakov, F. Delmotte, A. Giglia, P. Jonnard, Sc/SiC/Al multilayer optimization for Li K spectroscopy, Appl. Sci. 14 (2024) 956, https://doi.org/10.3390/app14030956.
[9] M. Terauchi, H. Takahashi, N. Handa, T. Murano, M. Koike, T. Kawachi, T. Imazono, M. Koeda, T. Nagano, H. Sasai, Y. Oue, Z. Yonezawa, S. Kuramoto, Ultrasoft-X-ray emission spectroscopy using a newly designed wavelength-dispersive spectrometer attached to a transmission electron microscope, J. Electron Microsc. 61 (1) (February 2012) 1–8, https://doi.org/10.1093/jmicro/dfr076.
[10] Y. Yamamoto, T. Murano, H. Onodera, N. Erdman, R. Matsuda, A. Matsuda, Time resolved SEM-SXES analysis for lithium material, Microsc. Microanal. 26 (S2) (2020) 68–70, https://doi.org/10.1017/S1431927620013276.
[11] J. Probst, H. Löchel, C. Braig, G. Achuda, S. Richter, A. Kempe, C. Seifert, T. Krist, A. Erko, WDSX-300: Ultra light element spectrometer, in: 17th European Workshop on Modern Developments and Applications in Microbeam Analysis, may 2023. Poland.
[12] K. Feser, *K*-shell fluorescence yield for metallic lithium and other light elements, Phys. Rev. Lett. 29 (14) (1972) 901–903, https://doi.org/10.1103/PhysRevLett.29.901. American Physical Society.
[13] K. Hassebi, K. Le Guen, N. Rividi, A. Verlaguet, P. Jonnard, Calculation of emission spectra of lithium compounds, X-Ray Spectrom. (2023) 1, https://doi.org/10.1002/xrs.3329.
[14] G.F. Bastin, H.J.M. Heijligers, Quantitative EPMA of the ultra-light elements boron through oxygen, in: A. Boekestein, M.K. Pavićević (Eds.), Electron Microbeam Analysis. Mikrochimica Acta vol. 12, Springer, Vienna, 1992.
[15] E. Brackx, P. Schweizer, Optimisation d’une microsonde WDS pour une détection du lithium, FR 2211207, Institut national de la propriété industrielle, 2022.
[16] CAMECA, Introduction to EPMA. https://www.cameca.com/products/epma/technique, 2017.
[17] A.J. Corso, M.G. Pelizzo, Extreme ultraviolet multilayer nanostructures and their application to solar plasma observations: a review, J. Nanosci. Nanotechnol. 19 (1) (2019) 532–545, https://doi.org/10.1166/jnn.2019.16477.
[18] D.L. Windt, IMD - software for modeling the optical properties of multilayer films, Comput. Phys. 12 (4) (1998) 360–370, https://doi.org/10.1063/1.168689.
[19] B. Henke, E. Gullikson, J. Davis, X-ray interactions: photoabsorption, scattering, transmission, and reflection at E = 50-30,000 eV, Z = 1-92, At. Data Nucl. Data Tables 54 (2) (1993) 181–342, https://doi.org/10.1006/adnd.1993.1013.
[20] P.T. Törmä, J. Kostamo, H. Sipilä, M. Mattila, P. Kostamo, H. Lipsanen, C. Laubis, F. Scholze, N. Nelms, B.J. Shortt, M. Bavdaz, Performance and properties of ultra-thin silicon nitride X-ray windows, IEEE Trans. Nucl. Sci. 61 (2014) 695–699, https://doi.org/10.1109/TNS.2014.2298434.
[21] J. Rafaelsen, T. Nylese, M. Bolorizadeh, V. Carlino, Windowless, silicon nitride window and polymer window EDS detectors: changes in sensitivity and detectable limits, Microsc. Microanal. 21 (S3) (2015) 1645–1646, https://doi.org/10.1017/S1431927615009009.
[22] P. Jonnard, C. Bonnelle, Cauchois and Sénémaud Tables of wavelengths of X-ray emission lines and absorption edges, X-Ray Spectrom. 40 (2024) 12–16, https://doi.org/10.1002/xrs.1293.
[23] P. Hovington, D. Drouin, R. Gauvin, CASINO: a new Monte Carlo code in C language for electron beam interaction — part I: description of the program, Scanning 19 (1) (2006) 1–14, https://doi.org/10.1002/SCA.4950190101.
[24] P. Hovington, V. Timoshevskii, S. Burgess, H. Demers, P. Statham, R. Gauvin, K. Zaghib, Can we detect Li K X-ray in lithium compounds using energy dispersive spectroscopy? Scanning 38 (2016) 571–578, https://doi.org/10.1002/sca.21302.
[25] H. Takahashi, T. Murano, M. Takakura, S. Asahina, M. Terauchi, M. Koike, T. Imazono, M. Koeda, T. Nagano, Development of soft X-ray emission spectrometer for EPMA/SEM and its application, IOP Conf. Ser. Mater. Sci. Eng. 109 (Feb. 2016) 012017, https://doi.org/10.1088/1757-899X/109/1/012017.
[26] K. Mukai, R. Kasada, K. Sasaki, S. Konishi, Occupied electronic states of Li in Li, Li2O2, and Li2O analyzed by soft X-ray emission spectroscopy, J. Phys. Chem. C 124 (17) (2020) 9256–9260, https://doi.org/10.1021/acs.jpcc.0c02885.
[27] S. Fukushima, T. Ogiwara, T. Kimura, S. Tanuma, A study of the appearance of Li Ka, IOP Conf. Ser. Mater. Sci. Eng. 7 (2010) 012010, https://doi.org/10.1088/1757-899X/7/1/012010.
[28] E.T. Arakawa, M.W. Williams, Radiative decay of core excitons in alkali halides, Phys. Rev. Lett. 36 (6) (1976) 333–336, https://doi.org/10.1103/PhysRevLett.36.333.
[29] E.J. Lavernia, T.S. Srivatsan, F.A. Mohamed, Strength, deformation, fracture behaviour and ductility of aluminium-lithium alloys, J. Mater. Sci. 25 (1990) 1137–1158, https://doi.org/10.1007/BF00585420.
[30] P. Donnadieu, The deviations of the Al6Li3Cu quasicrystal from icosahedral symmetry: a reminiscence of a cubic crystal, J. Phys. I 4 (5) (1994) 91–799, https://doi.org/10.1051/jp1:1994175.
[31] M. Khushaim, T. Boll, Experimental investigation of the early stage of precipitation on binary Al-Li, Al-Cu alloys and ternary Al-Li-Cu alloys by means of atom probe tomography, Open J. Metal 6 (2016) 25–44, https://doi.org/10.4236/ojmetal.2016.62003.
[32] K. Hassebi, N. Rividi, M. Fialin, A. Verlaguet, G. Godard, J. Probst, H. Löchel, T. Krist, C. Braig, C. Seifert, R. Benbalagh, R. Vacheresse, V. Ilakovac, K.L. Guen, P. Jonnard, X-Ray Spectrom. (2024) 1, https://doi.org/10.1002/xrs.3427.
[33] P. Schweizer, E. Brackx, P. Jonnard, Quantitative electron probe microanalysis of lithium in different materials including battery compounds, in: IUMAS-8, 8th Meeting of the International Union of Microbeam Analysis Societies, Jun 2023. Banff (Alberta), Canada, https://hal.science/cea-04185740v1.
[34] P. Schweizer, E. Brackx, P. Jonnard, Advances in quantitative electron probe microanalysis of lithium in different materials, in: Karim Zaghib, Philippe Jonnard, Raynald Gauvin (Eds.), LCPMR 2023 - International Workshop on the Characterisation and Quantification of Lithium. “From the Micro- to the Nano-Scale, from Mining to Energy”, Jun 2023. Paris, France, https://hal.science/hal-04219921.